J Neurophysiol 116: 1498–1506, 2016.
First published July 6, 2016; doi:10.1152/jn.00325.2016.

Glutamatergic drive facilitates synaptic inhibition of dorsal vagal motor neurons after experimentally induced diabetes in mice

Carie R. Boychuk and Bret N. Smith
Department of Physiology, University of Kentucky College of Medicine, Lexington, Kentucky

Submitted 21 April 2016; accepted in final form 1 July 2016

Boychuk CR, Smith BN. Glutamatergic drive facilitates synaptic inhibition of dorsal vagal motor neurons after experimentally induced diabetes in mice. *J Neurophysiol* 116: 1498–1506, 2016. First published July 6, 2016; doi:10.1152/jn.00325.2016.—The role of central regulatory circuits in modulating diabetes-associated glucose dysregulation has only recently been under rigorous investigation. One brain region of interest is the dorsal motor nucleus of the vagus (DMV), which contains preganglionic parasympathetic motor neurons that regulate subdiaphragmatic visceral function. Previous research has demonstrated that glutamatergic and GABAergic neurotransmission are independently remodeled after chronic hyperglycemia/hypoinsulinemia. However, glutamatergic circuitry within the dorsal brain stem impinges on GABAergic regulation of the DMV. The present study investigated the role of glutamatergic neurotransmission in synaptic GABAergic control of DMV neurons after streptozotocin (STZ)-induced hyperglycemia/hypoinsulinemia by using electrophysiological recordings in vitro. The frequency of spontaneous inhibitory postsynaptic currents (sIPSCs) was elevated in DMV neurons from STZ-treated mice. The effect was abolished in the presence of the ionotropic glutamate receptor blocker kynurenic acid or the sodium channel blocker tetrodotoxin, suggesting that after STZ-induced hyperglycemia/hypoinsulinemia, increased glutamatergic receptor activity occurs at a soma-dendritic location on local GABA neurons projecting to the DMV. Although sIPSCs in DMV neurons normally demonstrated considerable amplitude variability, this variability was significantly increased after STZ-induced hyperglycemia/hypoinsulinemia. The elevated amplitude variability was not related to changes in quantal release, but rather correlated with significantly elevated frequency of sIPSCs in these mice. Taken together, these findings suggest that GABAergic regulation of central vagal circuitry responsible for the regulation of energy homeostasis undergoes complex functional reorganization after several days of hyperglycemia/hypoinsulinemia, including both glutamate-dependent and -independent forms of plasticity.

GABA; glutamate; synapse; diabetes; vagus; brain stem

NEW & NOTEWORTHY

Results show that GABAergic synaptic regulation of central vagal motor neurons, which are responsible for regulating systemic energy homeostasis, undergoes complex functional reorganization in a type 1 diabetes model, including both glutamate-dependent and -independent forms of plasticity. These findings suggest a reorganization of brain stem circuitry regulating vagal motor output after several days of hyperglycemia/hypoinsulinemia that arises from, and could contribute to, visceral autonomic dysregulation in diabetes.

Address for reprint requests and other correspondence: B. N. Smith, Dept. of Physiology, Univ. of Kentucky College of Medicine, MS508 Chandler Medical Center, 800 Rose St., Lexington, KY 40536 (e-mail: bret.smith@uky.edu).

A BRAIN-MEDIATED MECHANISM of hyperglycemia was intimated long ago (Bernard 1855), but the role of the insulin-independent central regulatory circuits in modulating glucose homeostasis has only recently been under rigorous investigation (Breen et al. 2013; German et al. 2011; Ryan et al. 2014; Scarlett et al. 2016). Consistent with involvement of a "brain-centered glucose regulatory system" involving the central control of autonomic function (Schwartz et al. 2013), diabetes compromises several indexes of parasympathetic function, including altered gastric function (Rayner et al. 2001; Saltzman and McCallum 1983), reduced insulin secretion (Ahren 2000; Mussa and Verberne 2008; Yamatani et al. 1998), and dysregulated hepatic gluconeogenesis (Pocai et al. 2005b). Chronic autonomic dysfunction can promote development of type 2 diabetes (Carnethon et al. 2003), and compromised vagal function is directly linked to increased mortality (Thayer and Lane 2007). Although historically attributed to vagal neuropathy (Horowitz et al. 2002), compromised parasympathetic drive in diabetes often precedes degeneration of the vagus nerve (Mabe and Hoover 2011), implicating altered central vagal circuit function as a component of diabetic dysautonomia. Consistent with this hypothesis, neural signaling in brain areas that regulate the autonomic nervous system is altered after periods of chronic hyperglycemia in rodent models of diabetes (Bach et al. 2015; Blake and Smith 2014; Boychuk et al. 2015b; Browning 2013; Gao et al. 2012; Halmos et al. 2015; Roseberry et al. 2004; Zsombok et al. 2011). Additionally, the regulation of central autonomic circuits has been suggested as a potential therapeutic route for controlling diabetic hyperglycemia (Breen et al. 2013; Schwartz et al. 2013), even in rodent models of type 1 diabetes with uncontrolled hyperglycemia, and these effects are mediated by the vagus nerve (Breen et al. 2012; German et al. 2011; Pocai et al. 2005a; Yue et al. 2015). However, diabetes-associated effects on the brain stem circuitry that controls visceral homeostasis are not adequately understood.

The preganglionic parasympathetic motor neurons innervating most of the subdiaphragmatic viscera are located in the brain stem dorsal motor nucleus of the vagus (DMV). Together with sensory relay neurons in the nucleus tractus solitarii (NTS), the DMV regulates visceral function via the vagus nerve. Both glutamate and GABA mediate fast synaptic transmission in the DMV (Davis et al. 2004; Travagli et al. 1991). GABAergic neurotransmission arising from inhibitory neurons in the NTS (Davis et al. 2004; Frank et al. 2009; Glatzer and Smith 2005) is arguably the most prominent regulator of ongoing vagal motor neuron activity (Travagli et al. 2006). Consistent with the prominent role of GABA in regulating DMV neuron activity, $GABA_A$ receptor antagonist application

into the vagal complex significantly alters gastrointestinal and pancreatic function (Feng et al. 1990; Mussa and Verberne 2008; Washabau et al. 1995). Vagally mediated visceral functions related to energy homeostasis are thus tightly regulated by GABAergic signaling in the vagal complex.

This view, however, is somewhat simplistic, since the vagal complex comprises a heterogeneous population of neurons (Browning et al. 1999; Doyle et al. 2004; Glatzer et al. 2003) with high levels of interconnectivity (Davis et al. 2004; Glatzer and Smith 2005). In particular, glutamate acts both pre- and postsynaptically to facilitate GABA release in the DMV (Babic et al. 2011; Derbenev et al. 2006; Xu and Smith 2015). Acute glucose application modulates synaptic glutamate release in a population of NTS neurons (Wan and Browning 2008) and directly modulates GABAergic NTS neurons (Boychuk et al. 2015a; Lamy et al. 2014). After type 1 diabetes is experimentally induced, glutamate release in DMV neurons is significantly elevated (Bach et al. 2015; Zsombok et al. 2011). Previous reports suggest that synaptic GABAergic inhibition is not overtly altered after diabetes when glutamate receptors are blocked (Boychuk et al. 2015b), but the role dysregulated glutamate release plays in modulating GABAergic synaptic drive to the DMV is not known. The present study investigated glutamatergic drive to inhibitory circuits that regulate DMV activity in a murine model of type 1 diabetes. It was hypothesized that glutamate would prominently alter GABAergic, inhibitory synaptic transmission to DMV neurons from mice after chronic hyperglycemia and hypoinsulinemia. Synaptic variability and quantal analyses were utilized to further characterize glutamatergic facilitation of GABAergic IPSCs both under normal conditions and after disease.

METHODS

Animals

All experiments were performed on age-matched juvenile male (31.0 ± 1.0 g; 45 ± 2 days old) CD-1 mice (Harlan, Indianapolis, IN) housed in the University of Kentucky Division of Laboratory Animal Resources facilities under normal 14:10-h light-dark conditions, with food and water available ad libitum. The University of Kentucky Animal Care and Use Committee approved all animal procedures.

To induce type 1 diabetes with frank hyperglycemia, mice were fasted for 5–6 h before receiving an intraperitoneal injection of either streptozotocin (STZ; 200 mg/kg; Sigma-Aldrich, St. Louis, MO), to eliminate insulin-secreting pancreatic β-cells, or saline vehicle (0.1 ml). After injection, mice were returned to their home cages for 5–10 days. Blood glucose levels were monitored daily by tail snip (Onetouch Ultra; LifeScan, Chesterbrook, PA), and animals were used for experiments after ≥3 consecutive days of sustained blood glucose levels ≥300 mg/dl.

Electrophysiology

On the day of experimentation, mice were anesthetized with isoflurane to effect (i.e., lack of tail-pinch response) and decapitated while anesthetized. The brain stem was rapidly removed and submerged in ice-cold (0–4°C), oxygenated (95% O_2-5% CO_2) artificial cerebrospinal fluid (ACSF) with the following composition (in mM): 124 NaCl, 3 KCl, 26 $NaHCO_3$, 1.4 NaH_2PO_4, 11 glucose, 1.3 $CaCl_2$, and 1.3 $MgCl_2$. The osmolarity of all solutions was 290–305 mosmol/kg; pH 7.3–7.4. The brain stem was mounted, and slices (300 μm) were cut in the coronal plane using a vibratome. The slices were transferred to a holding chamber and incubated in warmed (30–33°C), oxygenated aCSF for 1 h before being transferred to a recording chamber mounted on the fixed stage of an upright microscope (BX51WI; Olympus, Melville, NY), where they were continuously superfused with warmed (30–33°C), oxygenated aCSF of identical composition to that used for slice preparation.

Whole cell patch-clamp recordings were performed under visual control using infrared illumination and differential interference contrast (IR-DIC) optics. Glass recording pipettes (2–5 MΩ; King Precision Glass, Claremont, CA) were filled with a solution containing the following (in mM): 130 Cs-gluconate, 1 NaCl, 5 EGTA, 10 HEPES, 1 $MgCl_2$, 1 $CaCl_2$, and 2–3 Mg-ATP; pH 7.3–7.4, adjusted with 5 M CsOH. Cs^+ was used as the primary cation carrier to block K^+ currents, which allowed consistent voltage clamp at depolarized membrane potentials and also diminished the contribution of postsynaptic $GABA_B$ receptors to inhibitory synaptic currents in recorded DMV neurons. $GABA_A$ receptor-mediated, inhibitory postsynaptic currents (IPSCs) were examined at a holding potential of 0 mV. Recordings were discarded if series resistance was >25 MΩ or changed by >20% throughout the course of the experiment; mean series resistance was 11.8 ± 0.8 MΩ. Electrophysiological signals were recorded using a Multiclamp 700B amplifier (Molecular Devices, Union City, CA), acquired at 20 kHz, low-pass filtered at 3 kHz, and stored to a computer using a Digidata 1440A digitizer and pCLAMP 10.2 software (Molecular Devices).

All drugs were bath applied until a steady state was reached (~10 min), at which time analysis was done. Drugs included the $GABA_A$ receptor antagonist bicuculline methiodide (BIC; 30 μM; R&D Systems, Minneapolis, MN), the ionotropic glutamate receptor antagonist kynurenic acid (KYN; 1 mM; Sigma-Aldrich), and the Na^+ channel blocker tetrodotoxin (TTX; 2 μM; Alomone Labs, Jerusalem, Israel).

Data Analysis

To determine drug effects on IPSCs, 2 min of continuous synaptic activity were analyzed offline using Clampex 10.2 (Molecular Devices) and MiniAnalysis 6.0.3. (Synaptosoft, Decatur, CA). All events were used to assess spontaneous IPSC (sIPSC) frequency, but only unitary events (i.e., single peak) were used for sIPSC amplitude and decay time measurements. Weighted decay time of the area [$\tau_{w(a)}$] was determined as the area of each IPSC divided by its peak amplitude. The coefficient of variation in sIPSCs was then determined for both amplitude and weighted decay time for each recording. The average number of sIPSCs used in the analysis of variability within a recording was 476 ± 50. To determine if sIPSC frequency predicted amplitude variability, neurons were classified as high frequency if their sIPSC frequency was greater than the group mean frequency.

Quantal analysis was completed as described previously (Edwards et al. 1990). For quantal analysis, the frequency of IPSC amplitudes was binned at 2 pA. Using OriginPro 9.1 (OriginLab, Northampton, MA), Gaussian curves were fitted to the peaks of these data. The IPSC amplitude at which each peak occurred was determined. The average difference between consecutive peaks was considered the quantal size for each recorded neuron.

For all experiments, only one cell was used per slice. Data are means ± SE. Statistical measurements were performed using GraphPad Prism 5 (GraphPad Software, La Jolla, CA). A one-way ANOVA (treatment × drug) with a Tukey's post hoc test was used to determine if KYN influenced sIPSC frequency means in unpaired analyses (i.e., drug effects in different neurons). For analyses of drug effects within a recording, a two-tailed paired Student's *t*-test was used to determine mean effects. A Kolmogorov-Smirnov (KS) test assessed individual neuronal responses to KYN application within a recording; a probability (*P*) value of <0.02 was considered significant for KS tests, which corresponded to a change in sIPSC frequency of ≥15%. For all other analyses, measurements done with no receptor antagonists present in the ACSF (nACSF) were compared between treatments using a two-tailed unpaired Student's *t*-test (i.e., saline- and STZ-

treated animals). Correlation analyses determined if electrotonic filtering contributed to differences in synaptic parameters or variability and if a relationship existed between sIPSC frequency and synaptic variability. Except for the KS test results, P values <0.05 were considered significant for all statistical analyses.

RESULTS

Characteristics of STZ-Induced Hyperglycemia

There was no difference in the age of animals used between groups (46 ± 3 days for saline-treated vs. 45 ± 3 days for diabetic animals; $P = 0.9$). The average blood glucose concentration of saline-treated CD-1 mice was 159.7 ± 5.7 mg/dl ($n = 22$). Mice were considered chronically hyperglycemic after maintaining >300 mg/dl blood glucose levels for at least 3 consecutive days following STZ treatment. The average blood glucose of STZ-treated mice on the day of the experiment was 480.6 ± 17.0 mg/dl ($P < 0.05$; $n = 20$). Animals were maintained in a hyperglycemic state for 3–7 days, with an average duration of 6 ± 0.4 days. By the day of experimentation, STZ-treated mice weighed less (28.1 ± 1.2 g) than saline-treated mice (33.8 ± 1.4 g; $P < 0.05$), which is similar to previous reports (Boychuk et al. 2015b; Rerup and Tarding 1969). Notably, peripheral STZ administration does not have neurotoxic effects in the DMV (Bach et al. 2015).

Glutamate Drives Inhibitory Synaptic Activity in the DMV

sIPSC frequency. A previous report found no differences in GABAergic IPSC frequency, amplitude, or decay time in murine DMV neurons after 3–7 days of continuous hyperglycemia in STZ-induced diabetes (Boychuk et al. 2015b). However, that study examined sIPSC parameters while ionotropic glutamate receptors were blocked, and glutamate receptor activation can profoundly modulate GABA release in the DMV (Babic et al. 2011; Bach et al. 2015; Derbenev et al. 2006; Xu and Smith 2015). Therefore, the following experiments determined if GABAergic neurotransmission was altered after 3–7 days of STZ-induced hyperglycemia when glutamate receptors were active within the slice. To do this, sIPSC parameters in DMV neurons from saline- and STZ-treated mice were examined with no receptor antagonists present in the ACSF (nACSF) and compared with measures performed while ionotropic glutamate receptors were blocked with KYN. Under nACSF conditions, neurons from eight STZ-treated mice had significantly higher sIPSC frequency (12.5 ± 2.7 Hz; $n = 21$ neurons) compared with neurons from 13 saline-treated mice (6.0 ± 1.1 Hz; $n = 26$ neurons; $P < 0.05$, ANOVA, Tukey's post hoc; Fig. 1). In six DMV neurons (3 from saline-treated controls and 3 from STZ-treated mice), BIC (30 μM) was applied to confirm that sIPSCs were indeed GABAergic; all sIPSCs were abolished after BIC application.

To further assess how glutamatergic neurotransmission influences sIPSCs in DMV neurons after chronic hyperglycemia, the within-recording effect of blocking ionotropic glutamate receptors was determined. In neurons from a different group of four saline-treated mice, the mean sIPSC frequency was not significantly different before (3.4 ± 0.6 Hz) and after KYN

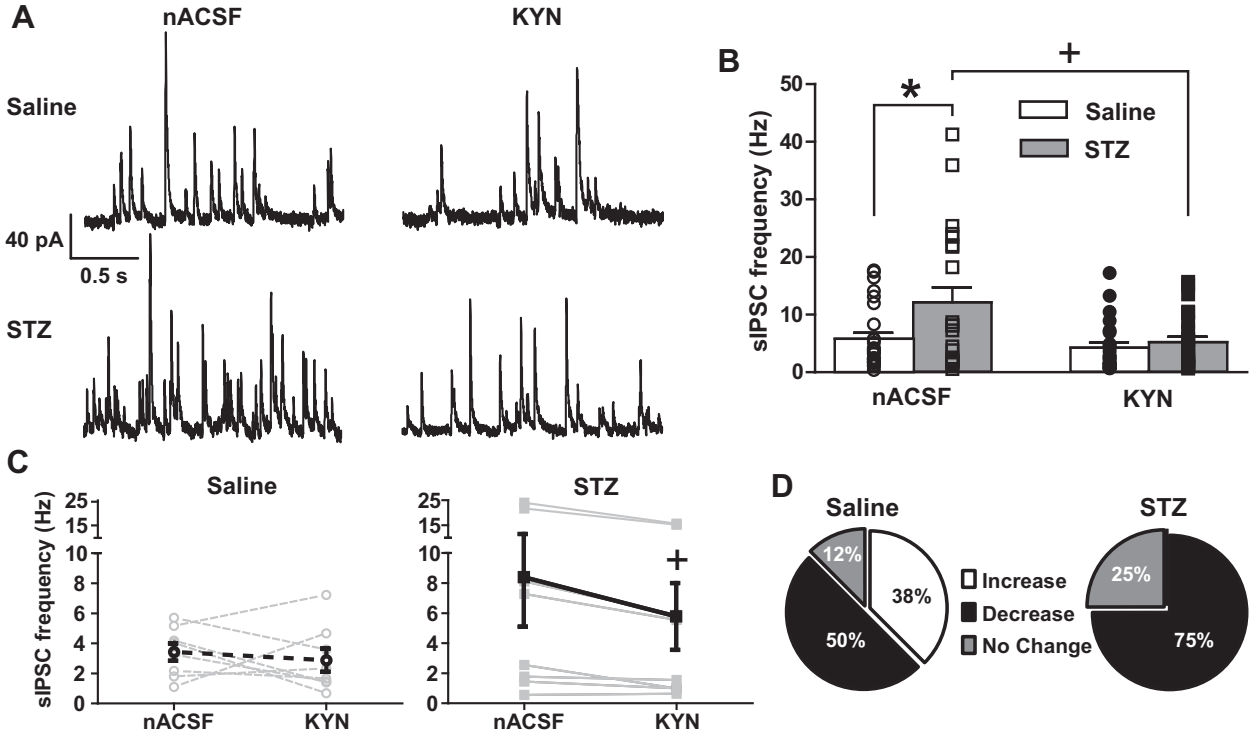

Fig. 1. Ionotropic glutamate receptor blockade abolishes sIPSC frequency differences in DMV neurons from mice with streptozotocin (STZ)-induced diabetes. *A*: representative traces showing sIPSCs in DMV neurons from saline- and STZ-treated mice in normal artificial cerebral spinal fluid (nACSF) and in the presence of kynurenic acid (KYN). *B*: mean sIPSC frequency differences between neurons from saline ($n = 26$)- and STZ-treated mice ($n = 21$) in nACSF and in the presence of KYN (saline: $n = 24$; STZ: $n = 25$). *C*: the effect of KYN application on sIPSC frequency from within-recording analysis in DMV neurons from saline ($n = 8$)- and STZ-treated mice ($n = 8$). *D*: pie graphs illustrating the effect on sIPSC frequency, expressed as the percentage of response types in each group, determined by within-recording Kolmogorov-Smirnov analysis. *$P < 0.05$, significant difference from saline-treated group. +$P < 0.05$, significant difference from nACSF.

application (2.9 ± 0.8 Hz; $n = 8$; $P = 0.55$; Fig. 1*C*). Individual neuronal responses were also examined using a KS test (Fig. 1*D*; $n = 8$); sIPSC frequency could be significantly ($P < 0.02$; >15% change) increased ($n = 3$; 28% of cells; 131.5 ± 96.4% change), decreased ($n = 4$; 50% of cells; −60.4 ± 9.7% change), or unchanged ($n = 1$; 12% of cells). In contrast, the mean sIPSC frequency in eight DMV neurons from three STZ-treated mice was significantly decreased after KYN application (5.8 ± 2.2 Hz) compared with nACSF (8.4 ± 3.3 Hz; $n = 8$; $P < 0.05$). This mean decrease was associated with a large percentage of neurons that responded to KYN with significantly decreased sIPSC frequency (75% of cells; 65 ± 22% change; $n = 6$; Fig. 1) and none with increased frequency. Therefore, chronic hyperglycemia results in an increase in glutamate's ability to drive GABAergic neurotransmission to the DMV. At the conclusion of the recording, neurons were voltage-clamped at −70 mV to confirm that excitatory PSCs (EPSCs) were completely blocked by KYN.

Miniature IPSC frequency. To determine the cellular location of glutamate receptor-dependent modulation of GABA release, the effect of KYN application was examined in the presence of TTX (2 μM) to block action potential firing (Fig. 2). In TTX, addition of KYN did not significantly alter miniature IPSC (mIPSC) frequency in neurons from saline-treated mice (TTX: 3.1 ± 1.6 Hz vs. KYN: 1.5 ± 0.5 Hz; $n = 7$; $P > 0.05$). The frequency of mIPSCs in individual DMV neurons from saline-treated mice was either increased ($n = 1$), decreased ($n = 1$), or unchanged ($n = 4$) by KYN application in the presence of TTX (Fig. 2*B*). Unlike for sIPSCs, mean mIPSC frequency in neurons from STZ-treated mice was unchanged after KYN application (TTX: 6.4 ± 2.2 Hz vs. KYN: 6.2 ± 2.7 Hz; $n = 7$; $P > 0.05$). The effect of KYN on mIPSC frequency in individual DMV neurons was variable (29% increased, 29% decreased, and 42% no change; Fig. 2*B*). Therefore, the ability of KYN to consistently decrease the frequency of GABAergic neurotransmission in DMV neurons from STZ-induced mice was abolished in the presence of TTX.

Other sIPSC parameters. Under normal recording conditions (i.e., no receptor antagonists), mean sIPSC amplitude in neurons from STZ-treated animals (41.9 ± 2.4 pA; $n = 21$) was not significantly different from that in neurons from the saline-treated group (41.8 ± 2.0 pA; $n = 26$; $P = 0.98$; Fig. 3*D*). Unlike a previous study of sIPSCs, which was performed in the presence of glutamate receptor blockade (Boychuk et al. 2015b), mean sIPSC weighted decay time in neurons from STZ-treated animals (6.5 ± 0.3 ms; $n = 21$) was significantly shorter than in neurons from the saline-treated group (7.4 ± 0.3 ms; $n = 26$; $P = 0.04$) when glutamate receptors were not blocked in the slice preparation.

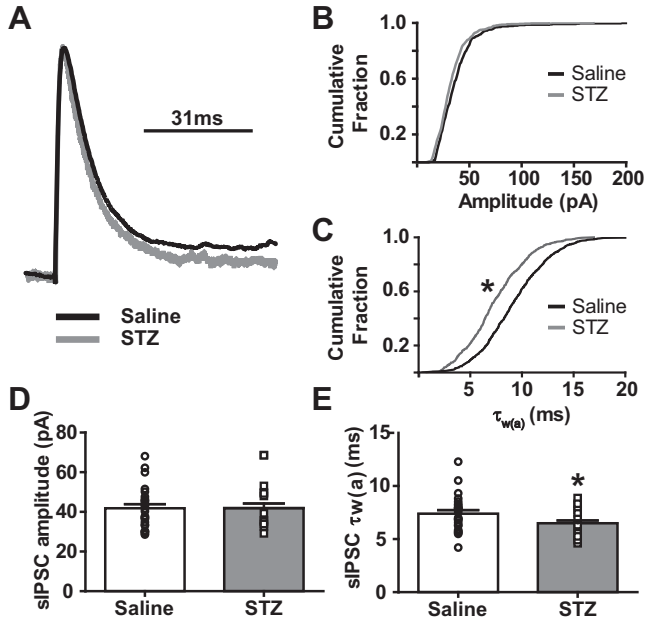

Fig. 3. STZ-induced diabetes shortens mean sIPSC weighted decay time [$\tau_{w(a)}$] but causes no change in mean amplitude. *A*: averaged traces of sIPSCs in DMV neurons from saline (black line)- and STZ-treated mice (gray line). Averaged traces were normalized for amplitude to demonstrate shortened $\tau_{w(a)}$. *B*: cumulative sIPSC amplitude fractions of individual DMV neurons from saline (black line)- and STZ-treated mice (gray line). *C*: cumulative $\tau_{w(a)}$ fraction of the same DMV neurons shown in *B* (saline treated, black line; STZ treated, gray line). *D* and *E*: mean sIPSC amplitudes (*D*) and $\tau_{w(a)}$ (*E*) from DMV neurons in saline ($n = 26$) and STZ ($n = 21$) groups. *$P < 0.05$, significant difference from saline-treated group.

Other mIPSC parameters. In the presence of TTX, mean mIPSC amplitude in neurons from STZ-treated animals (33.9 ± 1.8 pA; $n = 8$) was not significantly different from that in neurons from the saline-treated group (34.0 ± 1.5 pA; $n = 12$; $P = 0.99$). Mean mIPSC weighted decay time in neurons from STZ-treated animals (6.8 ± 0.4 ms; $n = 8$) was also not different from that in neurons from the saline-treated group (7.2 ± 0.3 ms; $n = 12$; $P = 0.44$).

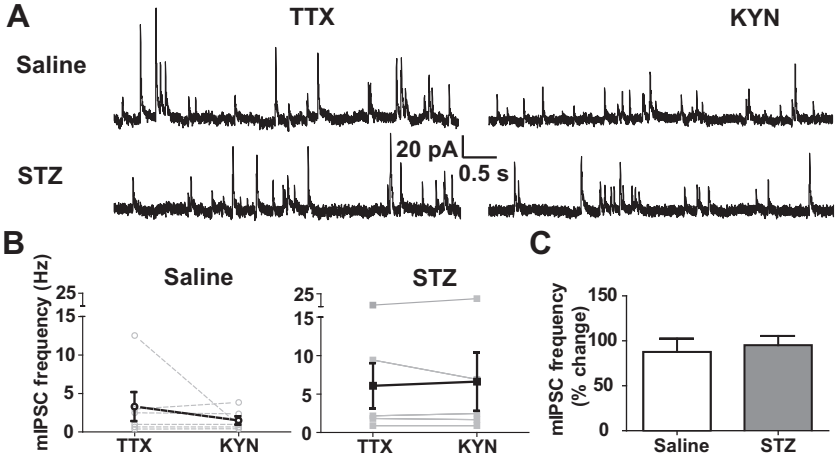

Fig. 2. Application of the sodium channel blocker tetrodotoxin (TTX) abolished the glutamate receptor-mediated effect on IPSC frequency. *A*: representative traces showing mIPSCs (TTX; 2 μM) in a DMV neuron from a saline-treated mouse (*top*) and an STZ-treated mouse (*bottom*) and the effect of KYN within the same neuron. *B*: the within-cell effect of KYN application on mIPSC frequency in DMV neurons from saline ($n = 6$)- and STZ-treated mice ($n = 6$). *C*: mean percent change in mIPSC frequency after bath application of KYN in saline- and STZ-treated groups.

Synaptic Variability in the DMV

sIPSC amplitude variability. In nASCF, the amplitude of sIPSCs in individual DMV neurons varied from just a few to several hundred picoamperes during the 2-min recording period. For example, the smallest measureable sIPSC in a single DMV neuron was 11.7 pA, and the largest event was 236.8 pA. This type of variability is illustrated in Fig. 4, *A* and *B*. Amplitudes were typically skewed toward smaller values (<75 pA; Fig. 4*B*). The average coefficient of variation for sIPSC amplitude in DMV neurons from saline-treated animals was 0.56 ± 0.02 (Fig. 5*B*). As demonstrated in Fig. 4*C*, this variability was not associated with changes in recording quality or sIPSC amplitude stationarity, since there was no relationship between sIPSC amplitude and time of recording ($R^2 = 0.004$). Neurons from STZ-treated animals demonstrated considerably greater amplitude variability compared with neurons from saline-treated animals. In the STZ-treated group, the average coefficient of variation was 0.68 ± 0.04 (Fig. 5*B*; $n = 21$; $P < 0.05$). To ensure that differences were not related to variability in electrotonic filtering between neurons from saline- and STZ-treated mice, the analysis of amplitude variation was restricted by rise time in two different ways. First, analysis was restricted only to events with rise times that fell one standard deviation away from the mean. A second analysis used only the fastest 50% of rise times. In all cases, the differences in variability remained between groups. A third, independent analysis to assess electrotonic filtering effects used a correlation analysis between the rise and decay times. The correlation between rise time and decay time was also not significant in cells from either saline-treated (mean P value = 0.31 ± 0.06; mean $R^2 = 0.01 \pm 0.006$) or STZ-treated mice (mean P value = 0.28 ± 0.07; mean $R^2 = 0.02 \pm 0.01$) or between groups ($P = 0.8$ for mean linear regression P value; $P = 0.6$ for mean R^2). Together, these data suggest that differences in variability between DMV neurons from saline- and STZ-treated were not mediated by differences in electrotonic filtering.

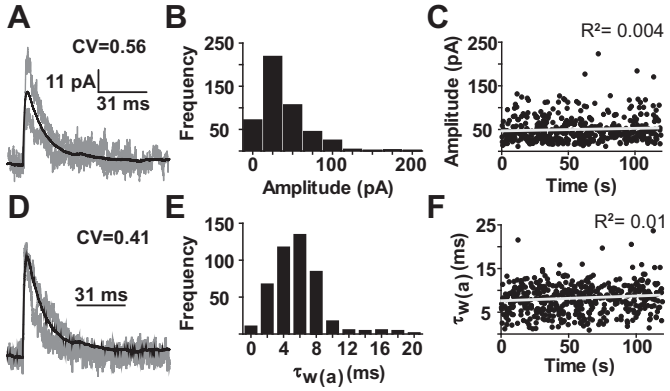

Fig. 4. Individual DMV neurons from control mice have considerable variability in sIPSC amplitude and weighted decay time [$\tau_{w(a)}$]. *A*: representative traces from one neuron from a saline-treated mouse demonstrating a significant degree of amplitude variability (CV) within an individual neuron (CV = 0.56). Gray traces represent 2 individual sIPSCs, with the overlaid average trace of all sIPSCs recorded in this neuron in black. *B*: frequency distribution of sIPSC amplitudes from the same neuron. *C*: stationarity of sIPSC amplitude over time ($R^2 = 0.004$). Each dot represents a single event. *D*: representative traces demonstrating $\tau_{w(a)}$ variability within another individual neuron from a saline-treated mouse (CV = 0.41). Gray traces represent 2 individual sIPSCs with the overlaid average trace in black. Traces were normalized for amplitude to demonstrate changes in $\tau_{w(a)}$. *E*: frequency distribution of sIPSC $\tau_{w(a)}$ from the recording shown in *D*. *F*: stability of $\tau_{w(a)}$ over time ($R^2 = 0.01$). Each dot represents a single event.

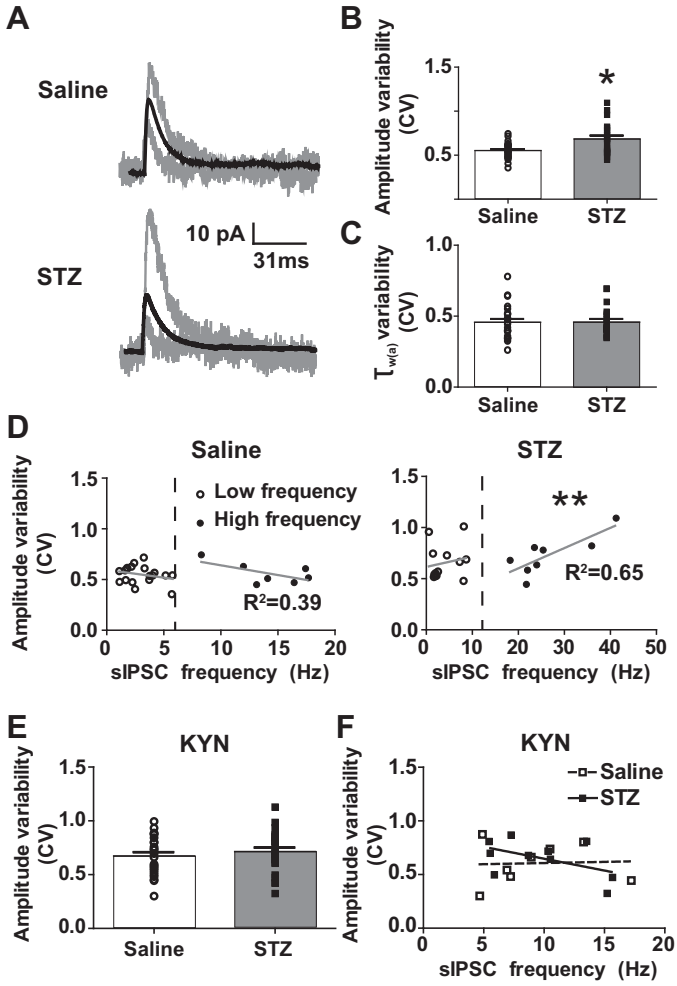

Fig. 5. sIPSC amplitude variability is increased in DMV neurons from STZ-treated mice. *A*: overlaid sIPSCs from DMV neurons in saline (*top*)- and STZ-treated mice (*bottom*). Gray traces represent 2 individual sIPSCs, with the overlaid average trace of all sIPSCs from this recording in black. *B*: mean sIPSC amplitude variability (CV) between neurons from saline ($n = 26$)- and STZ-treated mice ($n = 21$). *C*: mean sIPSC $\tau_{w(a)}$ variability is not different between groups. *D*: correlations between sIPSC amplitude variability and frequency in neurons from saline (*left*)- and STZ-treated mice (*right*), grouped as neurons with frequencies lower (○) or higher (●) than each group mean. *E*: mean sIPSC amplitude variability between neurons from saline ($n = 24$)- and STZ-treated mice ($n = 25$) after KYN application. *F*: correlations between sIPSC amplitude variability and frequency in neurons with highest frequency from saline (□) and STZ-treated groups (■) after KYN application. Note that each group axis in *D* is different for better visualization of differences. *$P < 0.05$, significant difference from saline-treated group. **$P < 0.05$, significant correlation between frequency and amplitude CV.

GABA$_A$ receptors are highly adaptable to ligand activation and increased receptor occupancy (i.e., through increased neurotransmitter release) should decrease amplitude variability (Faber et al. 1992; Frerking et al. 1995). Therefore, a correlation analysis between synaptic current amplitude variability and frequency of synaptic activity was used to determine if the high frequency of GABAergic sIPSCs related to changes in amplitude variability. Interestingly, sIPSC frequency in DMV neurons from STZ-treated animals with the highest sIPSC frequencies (greater than the mean frequency of 12.5 Hz) was positively correlated with amplitude variability ($P < 0.05$;

$R^2 = 0.65$; $n = 8$; Fig. 5*D*). A similar relationship did not exist for neurons from saline-treated mice (>6.0 Hz; $P > 0.05$; $R^2 = 0.39$; $n = 7$). Additionally, this relationship did not exist in either saline- or STZ-treated groups for individual DMV neurons with sIPSC frequencies lower than their respective group mean frequencies. KYN application eliminated the high-frequency groups, and therefore amplitude variability differences were not observed between neurons from saline- and STZ-treated mice (coefficient of variation = 0.67 ± 0.04 in saline-treated mice, $n = 24$, and 0.71 ± 0.04 in STZ-treated mice, $n = 25$; $P < 0.05$; Fig. 5*E*). Therefore, higher sIPSC frequency in DMV neurons predicted greater sIPSC amplitude variability from animals with chronic hyperglycemia, but not in control mice, and ionotropic glutamate receptor blockade eliminated the heightened sIPSC amplitude variability in STZ-treated mice (Fig. 5*F*).

sIPSC decay time variability. In each DMV neuron under nASCF conditions, the weighted decay time of sIPSCs varied considerably over the 2 min of recording examined. This variability is illustrated in Fig. 4, *D* and *E*. The weighted decay time variability was not associated with changes in the quality of the recording, since there was no change in decay time during recordings ($R^2 = 0.01$; Fig. 4*F*). The mean coefficient of variation for weighted decay time in DMV neurons from saline-treated animals was 0.46 ± 0.02 ($n = 26$; Fig. 5*C*). There was no difference in mean coefficient of variation for weighted decay time between saline- and STZ-treated mice (0.46 ± 0.02; $n = 21$; $P > 0.05$; Fig. 5*C*). No differences were determined when analysis was restricted by rise time, suggesting that variability was not mediated by differences in electrotonic filtering. Although mean decay time constant was faster in DMV neurons from STZ-treated, hyperglycemic/hypoinsulinemic vs. saline-treated control mice, decay time variability was similar for the two groups.

Quantal Analysis of GABAergic Neurotransmission

To determine if STZ-induced hyperglycemia altered the quantal size of GABA release per event, quantal analysis was completed. A representative histogram and its individual Gaussian curves from both treatment groups are demonstrated in Fig. 6*A*. In 11 neurons from saline-treated animals, the average quantal size from GABAergic terminals synapsing on the DMV was 16.15 ± 1.0 pA (Fig. 6*B*). This was not different in neurons from STZ-treated animals (14.56 ± 1.1 pA; $n = 7$; $P > 0.05$). Differences in mean frequency and amplitude variability of sIPSCs were therefore not predicted by a difference in quantal size.

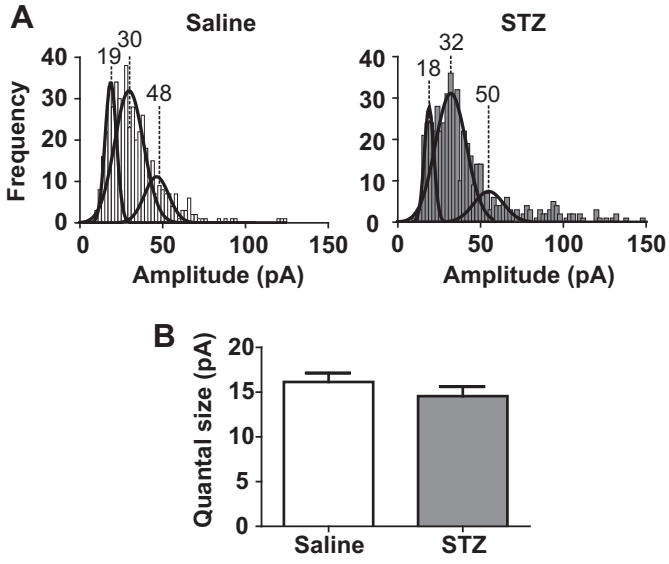

Fig. 6. Quantal sIPSC amplitude is not altered in DMV neurons from STZ-treated mice. *A*: distribution of sIPSC amplitudes in an individual DMV neuron from a saline-treated mouse and an STZ-treated mouse. Bin width is 2 pA. The thick line represents the Gaussian curves generated for each neuron with sIPSC amplitude noted above each peak. *B*: mean values of quantal sIPSC amplitude in DMV neurons from saline ($n = 11$)- and STZ-treated groups ($n = 7$).

DISCUSSION

The present study investigated the effect of glutamatergic neurotransmission on synaptic GABAergic currents in the DMV after the induction of chronic hyperglycemia in STZ-treated mice. A diabetes-associated increase in synaptic glutamate release has been reported previously in this model (Bach et al. 2015; Zsombok et al. 2011). The present results suggest that this plasticity contributes to glutamate-mediated modulation of GABAergic neurotransmission, even after glucose concentration is normalized in vitro. The facilitation of GABAergic synaptic activity was coupled with shorter weighted sIPSC decay times. Although sIPSCs in DMV neurons had significant variation in both amplitude and weighted decay time under nASCF conditions, sIPSCs in neurons from STZ-treated animals displayed significantly more variability in amplitude than those from saline-treated animals. These changes were not associated with altered quantal size, but elevated amplitude variability was strongly correlated with frequency in DMV neurons from STZ-treated animals with the highest sIPSC frequencies, and these differences were obviated by ionotropic glutamate receptor blockade. Taken together, these results suggest a significantly increased glutamate receptor-mediated facilitation of GABA release in the DMV, which contributes to significant increases in variability of synaptic GABAergic responses.

In nACSF, sIPSC frequency in neurons from STZ-treated animals was significantly elevated compared with that in neurons from saline-treated animals. The elevated sIPSC frequency was abolished in the presence of KYN, suggesting involvement of enhanced glutamate receptor-mediated excitation of GABAergic neurons presynaptic to the DMV in facilitating inhibitory drive to DMV neurons after chronic hyperglycemia. These data are consistent with previous reports demonstrating no differences in sIPSC frequency in the presence of KYN (Boychuk et al. 2015b) and those demonstrating elevated glutamatergic activity in both the DMV and NTS (Bach et al. 2015; Zsombok et al. 2011). TTX also normalized synaptic GABA release in DMV neurons from STZ-treated animals, indicating that the change in GABA release measured in the current study was action potential dependent. Interestingly, although unchanged by the induction of hyperglycemia/hypoinsulinema, results of quantal analysis suggested that GABAergic synapses on DMV neurons release two quanta on average, since mean mIPSC amplitude was approximately twice the mean quantal amplitude.

Together, these data imply that the glutamate receptors responsible for the facilitation of sIPSC frequency are located

on the soma-dendritic region of upstream GABA neurons within the slice. This input may arise from the NTS, which provides significant GABAergic projections to the DMV (Babic et al. 2011; Davis et al. 2004; Glatzer et al. 2003; Williams et al. 2007). The underlying source of the elevated glutamate activity could include increased sensitivity of NTS (or other) neurons to glutamate or increased glutamate release onto upstream GABA neurons contained within the slice, perhaps from vagal afferents. Primary viscerosensory vagal afferents from the gastrointestinal tract, which are implicated in the success of insulin-independent systemic glucose regulation and treatment of diabetes (Breen et al. 2012, 2013), synapse within the dorsal vagal complex, where they activate ionotropic glutamate receptors on postsynaptic NTS neurons (Andresen and Yang 1990; Smith et al. 1998; Zhao et al. 2015). Glutamate release from vagal primary afferents onto subsets of NTS neurons is increased when glucose concentration is elevated acutely in vitro (Boychuk et al. 2015a; Wan and Browning 2008). Under conditions of elevated glutamate release, which occurs in STZ-treated mice, NMDA and kainate, but not AMPA, receptors located on presynaptic terminals modulate GABA release in the DMV (Xu and Smith 2015). Additionally, in most NTS neurons, high-frequency activation of primary viscerosensory afferents promotes a sustained depolarization and action potential firing that is mediated by NMDA receptor-dependent mechanisms (Zhao et al. 2015). An increase in sensitivity of NMDA receptors on NTS neurons has been reported previously in STZ-treated, hyperglycemic mice (Bach et al. 2015). Thus diabetes may lead to increased glutamate release in the NTS and/or enhanced glutamate receptor-mediated responses in NTS neurons, resulting in a sustained increase in glutamate responsiveness of inhibitory projections from the NTS to the DMV.

In general, DMV neurons demonstrated large variations in both sIPSC amplitude and weighted decay time. IPSCs evoked in NTS neurons after tractus solitarius stimulation showed similarly large variability (McDougall and Andresen 2012). Amplitude variability of sIPSCs recorded from the soma can arise from differences within or between individual synaptic contacts of the recorded cell (Bekkers and Clements 1999). Although variation in synaptic parameters is associated with the concentration of GABA within the synaptic cleft (Faber et al. 1992; Nusser et al. 1997; Williams et al. 1998) and phosphorylation state of postsynaptic receptors (Jones and Westbrook 1997; Nusser et al. 1999; Poisbeau et al. 1999), diversity of $GABA_A$ receptor subunit composition is considered a prominent source of variability in synaptic signaling (Cherubini and Conti 2001; Eyre et al. 2012; Nusser et al. 1997). This type of subunit diversity has been demonstrated functionally in the DMV (Gao and Smith 2010a, 2010b), and responses of $GABA_A$ receptors mediating extra-/perisynaptic inhibition are functionally altered in STZ-treated mice (Boychuk et al. 2015b). Subtle subunit reorganization at synaptic receptors was also implied, since sIPSCs in DMV neurons from STZ-treated animals demonstrated altered subunit-specific agonist sensitivity. Given the diversity of $GABA_A$ receptor subtypes in the DMV, it is possible that shortened sIPSC decay times and increased amplitude variability in neurons from hyperglycemic/hypoinsulinemic mice reflect a modification of subunit composition, membrane location, or phosphorylation state of synaptic $GABA_A$ receptors in the DMV (Abramian et al. 2010; Boychuk et al. 2015b; Jones and Westbrook 1997; Krishek et al. 1994; Nusser et al. 1999; Poisbeau et al. 1999). Future studies should investigate further the diabetes-associated plasticity of GABA receptor function, since GABAergic inhibition potently modulates DMV neuron responses and parasympathetic visceral motor function (Babic et al. 2011; Davis et al. 2004; Feng et al. 1990; Mussa and Verberne 2008; Travagli et al. 2006; Washabau et al. 1995).

In neurons with high sIPSC frequency, the frequency correlated positively with amplitude variation in DMV neurons from STZ-treated, but not saline-treated mice, suggesting that glutamate-mediated facilitation of GABA release in the DMV might cause a functional alteration of postsynaptic $GABA_A$ receptor density in the DMV. $GABA_A$ receptor-mediated neurotransmission to DMV neurons arises from convergent inputs from multiple NTS neurons (Davis et al. 2004). Individual synaptic contacts express high levels of receptor heterogeneity across central synapses (Craig and Boudin 2001), so it is possible that changes in amplitude variability, but not mean amplitude, arise from hyperglycemia/hypoinsulinemia-induced plasticity within just a subset of these projections. These altered projections may arise selectively from GABAergic synapses located on the distal dendrites of DMV neurons, since amplitude variability increases with distance from the soma (Magee and Cook 2000).

Variability in sIPSC amplitude also results from differences in neurotransmitter concentrations within the synaptic cleft (Frerking et al. 1995), suggesting that elevated transmitter release should result in lower variability in sIPSC amplitudes (Hajos et al. 2000). GABA concentration seems likely to be higher in the DMV from hyperglycemic mice (i.e., inferred by increased sIPSC frequency), making the positive correlation between neurons with the highest frequency and amplitude variability somewhat surprising. It suggests, rather, that diabetes-related remodeling of DMV circuits may include an increased postsynaptic receptor density that exceeds that necessary to accommodate the greater ambient GABA concentration (see Fig. 7). A decrease in GABA concentration, relative to available receptors, would predict both decreased decay time and increased variation in amplitude of sIPSCs, which were

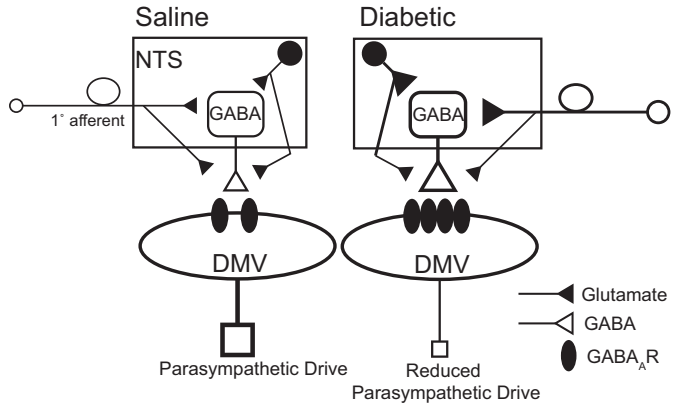

Fig. 7. Schematic depicting hypothesized changes in glutamate-mediated GABA release in the DMV in type 1 diabetes. Increased glutamatergic neurotransmission to GABAergic interneurons in the NTS results in chronically enhanced synaptic GABA release in the DMV. Paired with elevated functional $GABA_A$ receptor expression on DMV neurons, this may contribute to significantly diminished parasympathetic output to organ systems regulating energy homeostasis.

both detected in this study. It also implies a significant decoupling of the relationship between GABA release and receptor concentration in a large subset of neurons. Similar decoupling is suggested by the altered tonic GABA current density reported previously (Boychuk et al. 2015b). This decoupling could be mediated by or in addition to a reorganization of synaptic GABA receptor subunit composition after hyperglycemia/hypoinsulinemia. Therefore, diabetes may be related to an inappropriate postsynaptic mechanism of adaption to presynaptic GABA release at distal synapses.

Conclusions

After 3–7 days of continuous hyperglycemia/hypoinsulinemia, glutamate induced an action potential-dependent increase in synaptic GABA release when glucose concentration was standardized, suggesting a sustained functional plasticity of vagal circuits that outlasts the period of hyperglycemia. Alternatively, the changes could reflect an adaption in response to a return to normalized glucose concentration in these mice. This increased inhibition would be expected to inhibit parasympathetic control of subdiaphragmatic organs, including altered gastric function, diminished pancreatic secretory function, and suppressed braking of hepatic gluconeogenesis. This reduced parasympathetic output, especially the effect on hepatic gluconeogenesis, would be predicted to result in centrally mediated maintenance of hyperglycemia rather than an appropriate compensation. Changes in glutamatergic modulation of GABA release in the DMV might therefore contribute to the maintenance of a hyperglycemic state. The circuitry within the dorsal vagal complex should continue to be investigated as a potentially novel therapeutic target in the treatment of diabetes.

GRANTS

This work was supported by National Institutes of Health Grants R01 DK056132 and R21 HD079256.

DISCLOSURES

No conflicts of interest, financial or otherwise, are declared by the authors.

AUTHOR CONTRIBUTIONS

C.R.B. and B.N.S. conception and design of research; C.R.B. performed experiments; C.R.B. analyzed data; C.R.B. and B.N.S. interpreted results of experiments; C.R.B. prepared figures; C.R.B. drafted manuscript; C.R.B. and B.N.S. edited and revised manuscript; C.R.B. and B.N.S. approved final version of manuscript.

REFERENCES

Abramian AM, Comenencia-Ortiz E, Vithlani M, Tretter EV, Sieghart W, Davies PA, Moss SJ. Protein kinase C phosphorylation regulates membrane insertion of GABAA receptor subtypes that mediate tonic inhibition. *J Biol Chem* 285: 41795–41805, 2010.

Ahren B. Autonomic regulation of islet hormone secretion–implications for health and disease. *Diabetologia* 43: 393–410, 2000.

Andresen MC, Yang MY. Non-NMDA receptors mediate sensory afferent synaptic transmission in medial nucleus tractus solitarius. *Am J Physiol Heart Circ Physiol* 259: H1307–H1311, 1990.

Babic T, Browning KN, Travagli RA. Differential organization of excitatory and inhibitory synapses within the rat dorsal vagal complex. *Am J Physiol Gastrointest Liver Physiol* 300: G21–G32, 2011.

Bach EC, Halmos KC, Smith BN. Enhanced NMDA receptor-mediated modulation of excitatory neurotransmission in the dorsal vagal complex of streptozotocin-treated, chronically hyperglycemic mice. *PLoS One* 10: e0121022, 2015.

Bekkers JM, Clements JD. Quantal amplitude and quantal variance of strontium-induced asynchronous EPSCs in rat dentate granule neurons. *J Physiol* 516: 227–248, 1999.

Bernard C. *Lecçns de physiologie expérimentale appliquée a la médecine, faites au Collége de France*. Paris: J. B. Baillière, 1855.

Blake CB, Smith BN. cAMP-dependent insulin modulation of synaptic inhibition in neurons of the dorsal motor nucleus of the vagus is altered in diabetic mice. *Am J Physiol Regul Integr Comp Physiol* 307: R711–R720, 2014.

Boychuk CR, Gyarmati P, Xu H, Smith BN. Glucose sensing by GABAergic neurons in the mouse nucleus tractus solitarius. *J Neurophysiol* 114: 999–1007, 2015a.

Boychuk CR, Halmos K, Smith BN. Diabetes induces GABA receptor plasticity in murine vagal motor neurons. *J Neurophysiol* 114: 698–706, 2015b.

Breen DM, Rasmussen BA, Cote CD, Jackson VM, Lam TK. Nutrient-sensing mechanisms in the gut as therapeutic targets for diabetes. *Diabetes* 62: 3005–3013, 2013.

Breen DM, Rasmussen BA, Kokorovic A, Wang R, Cheung GW, Lam TK. Jejunal nutrient sensing is required for duodenal-jejunal bypass surgery to rapidly lower glucose concentrations in uncontrolled diabetes. *Nat Med* 18: 950–955, 2012.

Browning KN. Modulation of gastrointestinal vagal neurocircuits by hyperglycemia. *Front Neurosci* 7: 217, 2013.

Browning KN, Renehan WE, Travagli RA. Electrophysiological and morphological heterogeneity of rat dorsal vagal neurones which project to specific areas of the gastrointestinal tract. *J Physiol* 517: 521–532, 1999.

Carnethon MR, Golden SH, Folsom AR, Haskell W, Liao D. Prospective investigation of autonomic nervous system function and the development of type 2 diabetes: the Atherosclerosis Risk In Communities study, 1987–1998. *Circulation* 107: 2190–2195, 2003.

Cherubini E, Conti F. Generating diversity at GABAergic synapses. *Trends Neurosci* 24: 155–162, 2001.

Craig AM, Boudin H. Molecular heterogeneity of central synapses: afferent and target regulation. *Nat Neurosci* 4: 569–578, 2001.

Davis SF, Derbenev AV, Williams KW, Glatzer NR, Smith BN. Excitatory and inhibitory local circuit input to the rat dorsal motor nucleus of the vagus originating from the nucleus tractus solitarius. *Brain Res* 1017: 208–217, 2004.

Derbenev AV, Monroe MJ, Glatzer NR, Smith BN. Vanilloid-mediated heterosynaptic facilitation of inhibitory synaptic input to neurons of the rat dorsal motor nucleus of the vagus. *J Neurosci* 26: 9666–9672, 2006.

Doyle MW, Bailey TW, Jin YH, Appleyard SM, Low MJ, Andresen MC. Strategies for cellular identification in nucleus tractus solitarius slices. *J Neurosci Methods* 137: 37–48, 2004.

Edwards FA, Konnerth A, Sakmann B. Quantal analysis of inhibitory synaptic transmission in the dentate gyrus of rat hippocampal slices: a patch-clamp study. *J Physiol* 430: 213–249, 1990.

Eyre MD, Renzi M, Farrant M, Nusser Z. Setting the time course of inhibitory synaptic currents by mixing multiple $GABA_A$ receptor alpha subunit isoforms. *J Neurosci* 32: 5853–5867, 2012.

Faber DS, Young WS, Legendre P, Korn H. Intrinsic quantal variability due to stochastic properties of receptor-transmitter interactions. *Science* 258: 1494–1498, 1992.

Feng HS, Lynn RB, Han J, Brooks FP. Gastric effects of TRH analogue and bicuculline injected into dorsal motor vagal nucleus in cats. *Am J Physiol Gastrointest Liver Physiol* 259: G321–G326, 1990.

Frank JG, Jameson HS, Gorini C, Mendelowitz D. Mapping and identification of GABAergic neurons in transgenic mice projecting to cardiac vagal neurons in the nucleus ambiguus using photo-uncaging. *J Neurophysiol* 101: 1755–1760, 2009.

Frerking M, Borges S, Wilson M. Variation in GABA mini amplitude is the consequence of variation in transmitter concentration. *Neuron* 15: 885–895, 1995.

Gao H, Miyata K, Bhaskaran MD, Derbenev AV, Zsombok A. Transient receptor potential vanilloid type 1-dependent regulation of liver-related neurons in the paraventricular nucleus of the hypothalamus diminished in the type 1 diabetic mouse. *Diabetes* 61: 1381–1390, 2012.

Gao H, Smith BN. Tonic $GABA_A$ receptor-mediated inhibition in the rat dorsal motor nucleus of the vagus. *J Neurophysiol* 103: 904–914, 2010a.

Gao H, Smith BN. Zolpidem modulation of phasic and tonic GABA currents in the rat dorsal motor nucleus of the vagus. *Neuropharmacology* 58: 1220–1227, 2010b.

German JP, Thaler JP, Wisse BE, Oh IS, Sarruf DA, Matsen ME, Fischer JD, Taborsky GJ Jr, Schwartz MW, Morton GJ. Leptin activates a novel CNS mechanism for insulin-independent normalization of severe diabetic hyperglycemia. *Endocrinology* 152: 394–404, 2011.

Glatzer NR, Hasney CP, Bhaskaran MD, Smith BN. Synaptic and morphologic properties in vitro of premotor rat nucleus tractus solitarius neurons labeled transneuronally from the stomach. *J Comp Neurol* 464: 525–539, 2003.

Glatzer NR, Smith BN. Modulation of synaptic transmission in the rat nucleus of the solitary tract by endomorphin-1. *J Neurophysiol* 93: 2530–2540, 2005.

Hajos N, Nusser Z, Rancz EA, Freund TF, Mody I. Cell type- and synapse-specific variability in synaptic $GABA_A$ receptor occupancy. *Eur J Neurosci* 12: 810–818, 2000.

Halmos KC, Gyarmati P, Xu H, Maimaiti S, Jancso G, Benedek G, Smith BN. Molecular and functional changes in glucokinase expression in the brainstem dorsal vagal complex in a murine model of type 1 diabetes. *Neuroscience* 306: 115–122, 2015.

Horowitz M, O'Donovan D, Jones KL, Feinle C, Rayner CK, Samsom M. Gastric emptying in diabetes: clinical significance and treatment. *Diabet Med* 19: 177–194, 2002.

Jones MV, Westbrook GL. Shaping of IPSCs by endogenous calcineurin activity. *J Neurosci* 17: 7626–7633, 1997.

Krishek BJ, Xie X, Blackstone C, Huganir RL, Moss SJ, Smart TG. Regulation of $GABA_A$ receptor function by protein kinase C phosphorylation. *Neuron* 12: 1081–1095, 1994.

Lamy CM, Sanno H, Labouebe G, Picard A, Magnan C, Chatton JY, Thorens B. Hypoglycemia-activated GLUT2 neurons of the nucleus tractus solitarius stimulate vagal activity and glucagon secretion. *Cell Metab* 19: 527–538, 2014.

Mabe AM, Hoover DB. Remodeling of cardiac cholinergic innervation and control of heart rate in mice with streptozotocin-induced diabetes. *Auton Neurosci* 162: 24–31, 2011.

Magee JC, Cook EP. Somatic EPSP amplitude is independent of synapse location in hippocampal pyramidal neurons. *Nat Neurosci* 3: 895–903, 2000.

McDougall SJ, Andresen MC. Low-fidelity GABA transmission within a dense excitatory network of the solitary tract nucleus. *J Physiol* 590: 5677–5689, 2012.

Mussa BM, Verberne AJ. Activation of the dorsal vagal nucleus increases pancreatic exocrine secretion in the rat. *Neurosci Lett* 433: 71–76, 2008.

Nusser Z, Cull-Candy S, Farrant M. Differences in synaptic $GABA_A$ receptor number underlie variation in GABA mini amplitude. *Neuron* 19: 697–709, 1997.

Nusser Z, Sieghart W, Mody I. Differential regulation of synaptic $GABA_A$ receptors by cAMP-dependent protein kinase in mouse cerebellar and olfactory bulb neurones. *J Physiol* 521: 421–435, 1999.

Pocai A, Lam TK, Gutierrez-Juarez R, Obici S, Schwartz GJ, Bryan J, Aguilar-Bryan L, Rossetti L. Hypothalamic K_{ATP} channels control hepatic glucose production. *Nature* 434: 1026–1031, 2005a.

Pocai A, Obici S, Schwartz GJ, Rossetti L. A brain-liver circuit regulates glucose homeostasis. *Cell Metab* 1: 53–61, 2005b.

Poisbeau P, Cheney MC, Browning MD, Mody I. Modulation of synaptic $GABA_A$ receptor function by PKA and PKC in adult hippocampal neurons. *J Neurosci* 19: 674–683, 1999.

Rayner CK, Samsom M, Jones KL, Horowitz M. Relationships of upper gastrointestinal motor and sensory function with glycemic control. *Diabetes Care* 24: 371–381, 2001.

Rerup C, Tarding F. Streptozotocin- and alloxan-diabetes in mice. *Eur J Pharmacol* 7: 89–96, 1969.

Roseberry AG, Liu H, Jackson AC, Cai X, Friedman JM. Neuropeptide Y-mediated inhibition of proopiomelanocortin neurons in the arcuate nucleus shows enhanced desensitization in *ob*/*ob* mice. *Neuron* 41: 711–722, 2004.

Ryan KK, Tremaroli V, Clemmensen C, Kovatcheva-Datchary P, Myronovych A, Karns R, Wilson-Perez HE, Sandoval DA, Kohli R, Backhed F, Seeley RJ. FXR is a molecular target for the effects of vertical sleeve gastrectomy. *Nature* 509: 183–188, 2014.

Saltzman MB, McCallum RW. Diabetes and the stomach. *Yale J Biol Med* 56: 179–187, 1983.

Scarlett JM, Rojas JM, Matsen ME, Kaiyala KJ, Stefanovski D, Bergman RN, Nguyen HT, Dorfman MD, Lantier L, Wasserman DH, Mirzadeh Z, Unterman TG, Morton GJ, Schwartz MW. Central injection of fibroblast growth factor 1 induces sustained remission of diabetic hyperglycemia in rodents. *Nat Med* 22: 800–806, 2016.

Schwartz MW, Seeley RJ, Tschop MH, Woods SC, Morton GJ, Myers MG, D'Alessio D. Cooperation between brain and islet in glucose homeostasis and diabetes. *Nature* 503: 59–66, 2013.

Smith BN, Dou P, Barber WD, Dudek FE. Vagally evoked synaptic currents in the immature rat nucleus tractus solitarii in an intact in vitro preparation. *J Physiol* 512: 149–162, 1998.

Thayer JF, Lane RD. The role of vagal function in the risk for cardiovascular disease and mortality. *Biol Psychol* 74: 224–242, 2007.

Travagli RA, Gillis RA, Rossiter CD, Vicini S. Glutamate and GABA-mediated synaptic currents in neurons of the rat dorsal motor nucleus of the vagus. *Am J Physiol Gastrointest Liver Physiol* 260: G531–G536, 1991.

Travagli RA, Hermann GE, Browning KN, Rogers RC. Brainstem circuits regulating gastric function. *Annu Rev Physiol* 68: 279–305, 2006.

Wan S, Browning KN. D-glucose modulates synaptic transmission from the central terminals of vagal afferent fibers. *Am J Physiol Gastrointest Liver Physiol* 294: G757–G763, 2008.

Washabau RJ, Fudge M, Price WJ, Barone FC. GABA receptors in the dorsal motor nucleus of the vagus influence feline lower esophageal sphincter and gastric function. *Brain Res Bull* 38: 587–594, 1995.

Williams KW, Zsombok A, Smith BN. Rapid inhibition of neurons in the dorsal motor nucleus of the vagus by leptin. *Endocrinology* 148: 1868–1881, 2007.

Williams SR, Buhl EH, Mody I. The dynamics of synchronized neurotransmitter release determined from compound spontaneous IPSCs in rat dentate granule neurones in vitro. *J Physiol* 510: 477–497, 1998.

Xu H, Smith BN. Presynaptic ionotropic glutamate receptors modulate GABA release in the mouse dorsal motor nucleus of the vagus. *Neuroscience* 308: 95–105, 2015.

Yamatani K, Ohnuma H, Niijima A, Igarashi M, Sugiyama K, Daimon M, Manaka H, Tominaga M, Sasaki H. Impaired vagus nerve-mediated control of insulin secretion in Wistar fatty rats. *Metabolism* 47: 1167–1173, 1998.

Yue JT, Abraham MA, LaPierre MP, Mighiu PI, Light PE, Filippi BM, Lam TK. A fatty acid-dependent hypothalamic-DVC neurocircuitry that regulates hepatic secretion of triglyceride-rich lipoproteins. *Nat Commun* 6: 5970, 2015.

Zhao H, Peters JH, Zhu M, Page SJ, Ritter RC, Appleyard SM. Frequency-dependent facilitation of synaptic throughput via postsynaptic NMDA receptors in the nucleus of the solitary tract. *J Physiol* 593: 111–125, 2015.

Zsombok A, Bhaskaran MD, Gao H, Derbenev AV, Smith BN. Functional plasticity of central TRPV1 receptors in brainstem dorsal vagal complex circuits of streptozotocin-treated hyperglycemic mice. *J Neurosci* 31: 14024–14031, 2011.